

INVESTIGATION OF THE FLOW IN A RECTANGULAR CAVITY USING TOMOGRAPHIC AND TIME-RESOLVED PIV

C. Haigermoser*, F. Scarano**, M. Onorato*
 *Politecnico di Torino, **TU Delft

Keywords: tomographic PIV, cavity flows, 3-dimensional effects

Abstract

The flow in rectangular cavities with a laminar and a turbulent incoming boundary layer is investigated. Time-resolved planar PIV in a streamwise wall-normal plane provides information about the shear layer development, and especially about the influence of the cavity aspect ratio L/H on the instabilities in the flow. It is seen that at larger aspect ratios the impact of the flow in the downstream recirculation zone on the shear layer is stronger, leading to a higher energy content at low Strouhal numbers.

Tomographic time-resolved PIV is used to investigate the 3-dimensionality of the shear layer and the flow inside the cavity. The vortex shedding in the shear layer is seen to be rather 3-dimensional, especially in the downstream part of the cavity. 3D structures are also found inside the cavity, assuming the shape of horseshoe vortices.

1 Introduction

Cavity flows are of high interest in engineering applications, such as wheel wells, fuel vents or train windows. In these examples, a cavity can be a considerable noise source, and especially at high Mach numbers, it can also lead to significant structural loads. From an engineering point of view it is therefore necessary to deeply understand such flows and successively find means to control them.

Furthermore, cavity flows offer a broad range of fluid mechanical phenomena, like an unsteady shear layer developing from the leading edge,

vortex shedding, recirculation zones, instability and 3-dimensional effects. These phenomena can all be studied using such a simple geometry.

Most of the research up to date was carried out with 2-dimensional rectangular cavities. The first who gave a major contribution to the classification of flows in a rectangular cavity was Rossiter [24] (1964). He identified an acoustic feedback mechanism for certain cavities and flow regimes. This feedback mechanism can be described as follows:

A vortex is shed from the cavity leading edge and is convected downstream until it impinges onto the forward facing step, causing an acoustic pressure wave, which travels upstream and leads to instabilities in the shear layer and to the shedding of another vortex. Rossiter developed an empirical formula to predict the resulting oscillation frequencies, which is based on previous studies on edge tones (e.g. Powell [21] (1953), Powell [22] (1961)):

$$f = \frac{U_e(m - \gamma)}{L(M + 1/\kappa)} \quad (1)$$

where f is the frequency, U_e is the free-stream velocity, m is the integer mode number, γ is a factor accounting for the time lag between the passage of a vortex and the radiation of a pressure wave, L is the cavity length, M is the Mach number and κ is the ratio between convection velocity of the vortices and the freestream velocity. Rossiter and other researchers found good agreement between the formula and experimental results for $\gamma = 0.25$ and $1/\kappa = 1.75$. He further identified a resonant mode, which occurs when the flow oscillations excite an acoustic proper mode of the cavity.

The Rossiter model and similar models (see Rockwell and Naudascher [23], 1978), attempting to derive acoustic feedback mechanisms that predict the dominant frequencies, are adequately successful in the case of the shear regime flows. This flow regime is present at low aspect ratios L/H (cavity length/cavity depth $\lesssim 5$) and at reasonably high Mach and high Reynolds numbers, where the flow above the cavity is relatively undisturbed and the main unsteady flow feature is the convection of vortices in the shear layer (Tam C. and Block P. [29], 1978). Instead, for low Mach numbers, the flow oscillations are driven by convective waves rather than by shed vortices as found out by Sarohia [26] (1977) and by Chatellier et al. [4] (2004).

Another flow mode was found by Gharib and Roshko [9] (1987) at high L/H and when the length and/or depth of the cavity becomes large with respect to the upstream boundary layer thickness. In this so-called wake mode the flow behaves more like the wake of a bluff body, than a free shear layer. The flow becomes more violent and unsteady. A vortex that fills about the whole cavity is formed at the leading edge of the cavity and when it is large enough it is released at the trailing edge. In this regime the flow above the cavity is affected by the flow inside the cavity and the free-stream fluid is periodically directed into and out of the cavity (Larsson et al. [17] (2004)). This flow phenomena is connected with an high increase in drag.

Many studies have been performed to try to determine the range of parameters in which the different modes are expected to occur. The main parameter considered to predict the existence of peaks in the pressure spectra is the ratio between the cavity length and the incoming boundary layer momentum thickness L/θ (see Grace et al. [11] (2004)), where $L/\theta > 80$ is the condition which must apply in order to find oscillations in the cavity. However, experimental results are often in contrast, which may be due to the abundance of other geometrical and physical quantities involved, such as Reynolds number, Mach number, upstream boundary layer structure and three-dimensional effects.

For a general review of cavity flows, see Rockwell and Naudascher [23] (1978) and Komorath et al. [15] (1987). Here, only a few very recent experimental papers are referenced for their relevance to the present work, due to similar geometries tested and to the adopted measurements techniques (leading mainly to field data) and to give also a short (necessarily incomplete) view on the currently on-going work on the subject.

Grace et al. [11] (2004) measured mean and turbulent flow fields in a shallow cavity, $L/H = 4$, subject to low Mach number, considering the cases of both laminar and turbulent upstream boundary layers. Different upstream flow conditions were explored, $L/\theta = 130$ and 190 for the laminar case and $L/\theta = 78$ and 86 for the turbulent case. The corresponding Re_δ were respectively 2892, 3949, 6318, 12627. In spite of the high values of L/θ in their experiments, no self-sustained oscillations were observed. They show and discuss interesting comparisons with data of previous studies for resonating cavities. Flow field measurements were taken by using a cross-wire anemometer and two-component laser Doppler Velocimetry. A similar cavity flow pattern was found for the laminar and turbulent cases with a difference in the location of the main recirculation zone, which in the case of a laminar upstream boundary layer was found closer to the trailing edge and showed 35% stronger vorticity. In addition, the distribution of the Reynolds shear stress was similar, with some difference in the location of its maximum value. Chatellier et al. [4] (2004) conducted theoretical and experimental investigations for rectangular resonating cavities of different sizes, in low Mach number flows, finding good agreement between the data obtained with the two techniques. The Reynolds number based on the cavity length was typically from $Re_L = 105$ to $3 \cdot 10^5$. Results are mainly shown for $L/H = 1$. PIV measurements, phase locked with the oscillation cycles via a wall mounted microphone, revealed that the cavity flow was not governed by the periodic shedding of coherent structures from the leading edge, but by self-sustained oscillations of the unstable shear layer. Acoustic modes were also

individuated by means of microphones located in different positions.

PIV data was analyzed by Ukeiley and Murray [30] (2005) to yield mean flow characteristics, vorticity field information, and two-point statistics, for cavities with $L/H = 5.16$ and $L/H = 1.49$ at $M = 0.2$. The upstream turbulent boundary layer was characterized respectively by $L/\theta = 58.3$ and $L/\theta = 46.4$. Tonal oscillations were observed only for the deep cavity. Ukeiley and Murray [30] (2005) also performed hot-wire measurements combined with wall pressure measurements to obtain correlations between velocity and pressure fluctuations. They further combined PIV data with surface pressure measurements through the application of quadratic stochastic estimation to predict the time dependent behavior of the velocity field. This strategy was demonstrated to be an effective tool to represent the time dependent phenomena of the velocity field, even though the velocity measurements were not time resolved. The estimated time-dependent velocity field was able to show the breathing action of the velocity field occurring in both cavities studied, enlightening the different mechanisms driving the flapping motion in the two cavities.

Ozsoy et al. [19] (2005) studied a $L/H = 4$ cavity with a laminar incoming boundary layer, at very low Mach number, examining three Reynolds numbers ($Re_H = 4000, 9000$ and 13000). PIV data were analyzed to characterize the vortical flow in the shear layer in terms of probability density function of vortex location, vortex size and vortex circulation. They observed the sensitivity of the mean and turbulent flow velocities and of the vortex characteristics on the Reynolds number. In spite of the large values of L/θ , ranging from 114 to 160, no feedback mechanism involving regular flow self-sustained oscillations was observed.

The absence of self-sustained oscillations was also revealed by the PIV investigation conducted by Ashcroft and Zhang [2] (2005) on cavities having the ratio $L/H = 2, 3$ and 4 , at different low subsonic flow speeds. Also in their case the ratio L/θ was high, ranging from 127 to 270.

To provide insight into the instantaneous large scale and small scale flow structures, a Galilean decomposition and a LES decomposition were respectively applied to the individual velocity field data sets. They observed that the stochastic structures induce a strong intermittency into the flow that prevents the development of strong self-sustained oscillations. A statistical two-point correlation analysis revealed that the integral scale of the flow structures grows linearly in the shear layer across the cavity opening.

So far 3-dimensional effects were not studied extensively as the transverse modes contribute only little to the acoustic emission of the cavity. However, the 3D flow inside the cavity may condition and influence the noise generating mechanisms. Faure et al. [7] (2007) studied recently 3D effects in different rectangular cavities with a laminar incoming boundary layer by flow visualization. First, they found by visualizations parallel to the wall the presence of jets inside the cavity, coming from the lateral boundaries, for all tested shallow cavity aspect ratios ($L/H=1, 1.5$ and 2). Further, pairs of vortices were found along the backward and forward facing step. These vortex pairs were seen to move from the center towards the cavity lateral side walls. Simultaneous visualizations of two wall-normal streamwise planes suggested that the vortex shedding from the cavity leading edge is 2-dimensional.

The interest in the aeroacoustic aspects of cavity flows has increased during the last few years, mainly in the aeronautic and automotive industry, primarily because of customer comfort. In order to search for sound sources that can be generated by the flow inside and around the cavity, the unsteady nature of the flow needs to be observed. The spatial complex nature of the shear layers and the complex array of evolving scales made point-wise measurements and time or phase averaged data not fully adequate to describe their dynamics and complexity.

The aim of the present study is therefore to investigate the structure and dynamics of an unsteady turbulent shear layer past a nominally 2-dimensional, shallow, open, rectangular cavity,

at low speed, performing optical space and time-resolved measurements, using Particle Image Velocimetry (PIV). This measurement method allows the observation of the full 2D/3D flow field and the evolution of the flow structures in time. Cavities with aspect ratios $L/H=2, 3$ and 4 with a turbulent and a laminar incoming boundary layer are investigated.

2 Experimental facilities and measurement techniques

The following experiments were carried out for this study:

- a) Time-resolved planar PIV measurements in streamwise wall-normal and wall-parallel planes with a laminar upstream boundary layer (Exp 1-3).
- b) Time-resolved planar PIV measurements in streamwise wall-normal planes with a turbulent upstream boundary layer (Exp 4).
- c) Tomographic PIV measurements with a turbulent upstream boundary layer (Exp. 5).
- d) Time-resolved tomographic PIV measurements with a laminar upstream boundary layer (Exp. 6).

Table 1 gives an overview of the conducted experiments.

2.1 Time-resolved planar PIV measurements

The planar PIV time-resolved experiments were carried out in a water tunnel at the Politecnico di Torino with a test section of $350 \times 350 \text{ mm}^2$. Fig. 1 shows the cavity model in the tunnel test section.

The cavity depth H was 10 mm . The cavity aspect ratios L/H for the cases of the laminar incoming boundary layer were $2, 3$ and 4 . The ratio L/θ ranged from 33 to 67 , where the latter is close to a reference value which was determined to be significant for the onset of oscillations and which is $L/\theta > 80$ (see Grace et al. [11]). In case of the turbulent upstream boundary layer

Table 1 Experimental setup. Overview.

	Exp 1	Exp 2	Exp 3
PIV	planar, time-resolved	planar, time-resolved	planar, time-resolved
State BL	laminar	laminar	laminar
$\delta [mm]$	2	1.5	2
$U_e [m/s]$	0.36	0.26	0.36
$\delta^* [mm]$	1.46	1.2	1.46
$\theta [mm]$	0.6	0.5	0.6
Re_L	14400	10400	14400
Re_θ	216	130	216
L/H	4	3	2
W/L	8.75	11.6	17.5
L/θ	67	60	33
	Exp 4	Exp 5	Exp 6
PIV	planar, time-resolved	tomographic, not time-resolved	tomographic, time-resolved
State BL	turbulent	turbulent	laminar
$\delta [mm]$	21	22.5	3.5
$U_e [m/s]$	0.4	12	0.49
$\delta^* [mm]$	3.4	3.9	1.09
$\theta [mm]$	2.24	2.8	0.422
Re_L	18500	32000	19600
Re_θ	1041	2240	206
L/H	4	4	3
W/L	8.75	10	11.5
L/θ	18	14	110

one aspect ratio $L/H = 4$ was tested. The turbulent boundary layer was tripped with a fetch of sand paper, placed 180 cm upstream of the cavity (the upstream plate was elongated for this experiment) and was fully developed when it reached the cavity. The thickness of the boundary layer was $\delta = 21 \text{ mm}$. Thus, the boundary layer thickness was 2.1 times larger than the cavity depth H . The ratio of the cavity length L over θ was $L/\theta = 18$.

The experiments were conducted in planes normal to the wall at the center between the lateral confines of the cavity, and in planes parallel to the wall at different levels inside and slightly outside the cavity. In case of the vertical measurements, the field of view covered the whole cavity and the complete boundary layer up to the region of undisturbed flow outside the boundary layer. The field of view in the horizontal measurements captured the full longitudinal extension of the cavity. The PIV setup consisted of a continuous Spectra-

INVESTIGATION OF THE FLOW IN A RECTANGULAR CAVITY USING TOMOGRAPHIC AND TIME-RESOLVED PIV

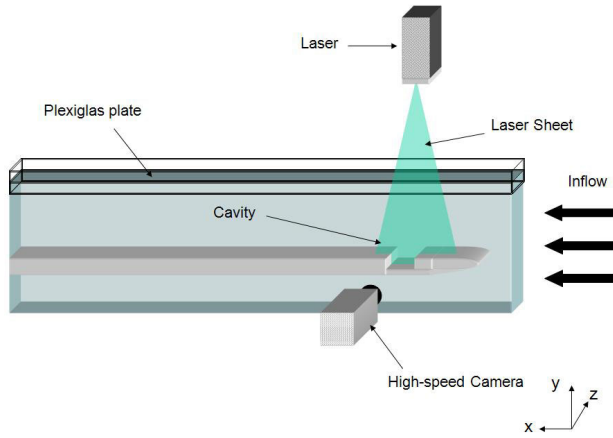


Fig. 1 Experimental setup exp. 1-3.

Physics Argon-Ion laser with a maximum emitted beam power of 6 W , illuminating the measurement plane with a laser light sheet, 1 mm thick. The flow was seeded with hollow glass spheres with a nominal diameter of $10\ \mu\text{m}$. The particles image size was approximately 3 pixels at $f_{\#} = 2.8$.

The PIV images were acquired using a Dantec MKIII CMOS camera with a resolution of 1280×1024 pixels and a maximum recording rate at full resolution of 1000 fps which was also the acquisition rate used in the experiment. The camera has an internal memory of 4 GB , which limited the acquisition time for the mentioned acquisition rate at full resolution and at single exposure to 3.2 seconds giving 3200 images. Statistically independent measurements were performed taking only every 100th and 101st image, thus an effective acquisition rate of 10 Hz was performed. The number of acquired image pairs for the statistics was 3000. Two successive images were cross-correlated to obtain the velocity field using a multigrid algorithm provided by the DAVIS 7.2 software by LaVision with an initial interrogation window size of 128×128 pixels and a final interrogation window size of 32×32 pixels with a 50% overlap, applying sub-pixel refinement and window deformation. Hence, the velocity represented by one vector depends on the field of view which depends on the tested cavity length. For the case of the cavity with $L/H=4$

one vector corresponds to the velocity in a spatial area of $1.2 \times 1.2\text{ mm}^2$ and diminished to half of that for the cavity with $L/H=2$.

The error in measuring the flow velocity with PIV depends on the particle image size, the particle image density and the velocity gradient. Based on the present images the error in measuring the displacement can be estimated being less than 0.1 pixels. With a displacement from one image to the successive one of more than 10 pixels in the outer flow and about half of it in the shear layer, the error in measuring the velocity can be estimated to be less than 2%.

2.2 Tomographic PIV measurement

The tomographic PIV experiment (not time-resolved, Exp. 5) was conducted at the Aerodynamics Laboratories of TU Delft in a open wind tunnel with a test section area of $400 \times 400\text{ mm}^2$. It is complementary to Exp. 4, even if the Reynolds numbers are different, but the incoming boundary layer is in both cases thick, which is the main feature influencing the flow, as it will be shown.

A flat plate was placed upstream of the cavity to control the development of the upstream boundary layer, which was tripped at the flat plate leading edge with a strip of sand paper. The plate was placed into the test section center so that the cavity was situated right at the test section exit in order to enable optical access, see Fig. 2.

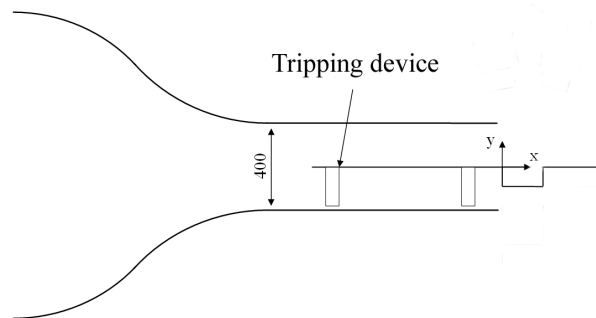


Fig. 2 Experimental setup of Exp. 5.

The cavity upstream boundary layer was fully turbulent with the characteristics as shown in table 1. The ratio of the boundary layer thickness

and the cavity depth was $\delta/H = 2.5$. The ratio $L/\theta = 14$. The experimental setup is shown in Figs.3a and 3b. The experiment was carried out using 4 cameras (PCO Sensicam QE CCD; 1376x1040 pixels) all inclined 10° from the wall normal direction. The cameras were equipped with Nikon lenses with a focal length of 60mm at $f_\# = 8$. The measurement volume, was illuminated by BigSky CFR200 Nd:YAG laser with a maximum energy of 200 mJ per pulse and a maximum repetition rate of 30 Hz. The laser light sheet was 10 mm thick. The measured volume was located at $-5 \text{ mm} < y < 5 \text{ mm}$, covering the cavity shear layer. Oil droplets with a diameter of $10 \mu\text{m}$ were used to seed the flow, yielding a particle image diameter of approximately 3 pixels. Before correlating the images, a background image was subtracted from the PIV images to reduce reflections coming from the cavity walls, the particle image intensity was equalized and pixel noise was reduced by Gaussian smoothing. The volumes were reconstructed using 5 MART iterations (Multiplicative Algebraic Reconstruction Technique, [5]) at a pixel to voxel ratio of 1, leading to a volume of $1094 \times 1088 \times 224$ voxels (24 voxels per mm). The reconstructed volumes were cross-correlated using the VODIM software developed at the TU Delft. The final interrogation volume size was $30 \times 30 \times 30$ voxels ($1.6 \times 1.6 \times 1.6 \text{ mm}^3$) at an overlap of 50%.

The error of a tomographic PIV setup was assessed by Elsinga et al. [5], where the displacement error is estimated to lie between 0.1 and 0.16 voxels. It is mentioned that this error can still be improved applying a self-calibration procedure, as it was done in the present case. Anyway, considering the above error level, the error in measuring the velocity in the present case can be estimated to be lower than 2% at a displacement of the particles of about 10 voxels within an image pair inside the shear layer.

2.3 Time-resolved tomographic PIV measurement

The time-resolved tomographic PIV measurements were carried out at the Laboratory for Aero

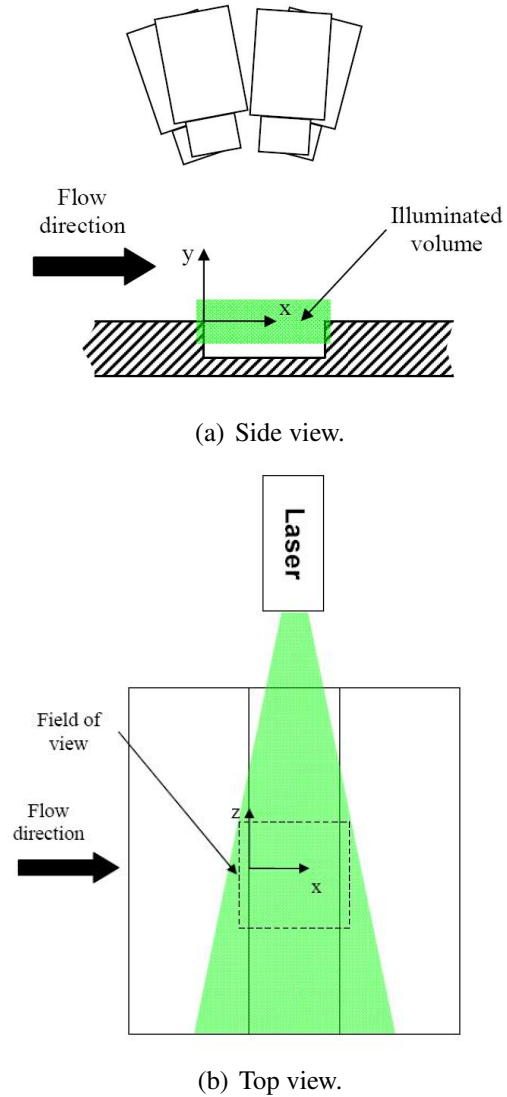


Fig. 3 Experimental setup Exp. 5.

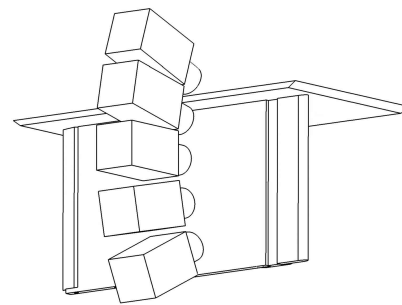


Fig. 4 Experimental setup Exp. 6.

INVESTIGATION OF THE FLOW IN A RECTANGULAR CAVITY USING TOMOGRAPHIC AND TIME-RESOLVED PIV

& Hydrodynamics of the TU Delft in a water tunnel with a test section area of $600 \times 600 \text{ mm}^2$. These measurements are complementary to the Exps. 1-3, see above. The Plexiglas plate with the cavity was placed vertically inside the tunnel 150 mm away from the tunnel wall. The cavity was confined at one side by the tunnel bottom wall and from the other side by a Plexiglas plate, which was placed such that the water did not pass over or under the plate.

The freestream velocity was 0.49 m/s and the incoming boundary layer was laminar, see Table 1. The flow was seeded using hollow polyamid spheres (Degussa, VESTOSINT 2157) with a nominal diameter of $50 \text{ }\mu\text{m}$. The tomographic PIV setup consisted of 2 Photron Highspeedstar5 and 3 Photron Highspeedstar6 cameras with 1024×1024 pixels and a maximum acquisition rate of 3000 fps . The cameras were aligned with the cavity as shown in Fig. 4. They were equipped with objectives having a focal length of 105 mm . The $f\#$ was adjusted to 22, giving a particle image diameter of 3 pixels. The laser light sheet was 20 mm thick and was introduced from the top through the top plate along the cavity. The light was produced by a Quantronix Darwin Duo laser emitting more than 50 mJ per pulse, depending on the pulse frequency. The maximum obtainable frequency is 20 kHz . The field of view had a size of $50 \times 50 \times 20 \text{ mm}^3$ and included all the cavity plus 7 mm outside the cavity. The following procedures for the PIV analysis were carried out using the DAVIS 7.4 software by LaVision. The images were pre-processed applying particle image intensity equalization, subtracting the sliding minimum with a kernel of 11×11 pixels and applying a Gaussian smoothing with a kernel of 3×3 pixels. The resulting images had a good contrast between the particles and the background. Successively, the tomographic reconstruction was performed using 5 MART iterations, with a pixel to voxel ratio of 1 giving a reconstructed volume, which consisted of $1197 \times 1118 \times 432$ voxels. Thus the spatial resolution was 20 voxels/mm . The reconstructed volumes were cross-correlated using an adaptive algorithm with a starting interrogation window size

of $128 \times 128 \times 40$ voxels and a final interrogation window size of $40 \times 40 \times 32$ voxels with an overlap of 50%. The obtained vector field had $55 \times 52 \times 20$ vectors, each vector representing the velocity in a spatial area of $2 \times 2 \times 1.6 \text{ mm}^3$. The applied acquisition rate for this experiment was 1000 fps leading to a displacement of the particles within two successive snapshots of about 12 voxels in the shear layer.

The error in measuring the displacement with this tomographic PIV setup is slightly lower than with the one in air as described above, as the image quality respectively the signal to noise ratio in water is much better than in air. Applying further image preprocessing and self-calibration, the error in measuring the displacement is estimated to be 0.1 voxels, which yields an error in measuring the velocity with the above mentioned displacement of less than 1%.

3 Results and discussion

In the following section, the discussion of the results will be mainly based on data obtained from the planar PIV measurements (Exp. 1 - 4). The tomographic PIV data (Exp. 5 and 6) is used to support the observations in the 2D planes.

3.1 Mean and turbulent quantities

The results of Experiment 4 can be found in Haigermoser et al. [12] (2008) in more detail. It will be summarized here, in order to compare them with the experiments 1-3.

First, the mean and turbulent flow characteristics within the cavity are presented. Figs.5a and 5d show the mean flow in the cavities with aspect ratio $L/H=4$ respectively with laminar and turbulent incoming boundary layer. The flow pattern is very similar, consisting of a large clockwise re-circulating zone covering more than the downstream half of the cavity. A weaker counter-re-circulating zone (secondary vortex) is evident near the upstream corner, driven by the primary region of recirculation. The streamlines in Figs. 5a and 5d indicate further the impingement of the mean shear layer onto the upper part of the front

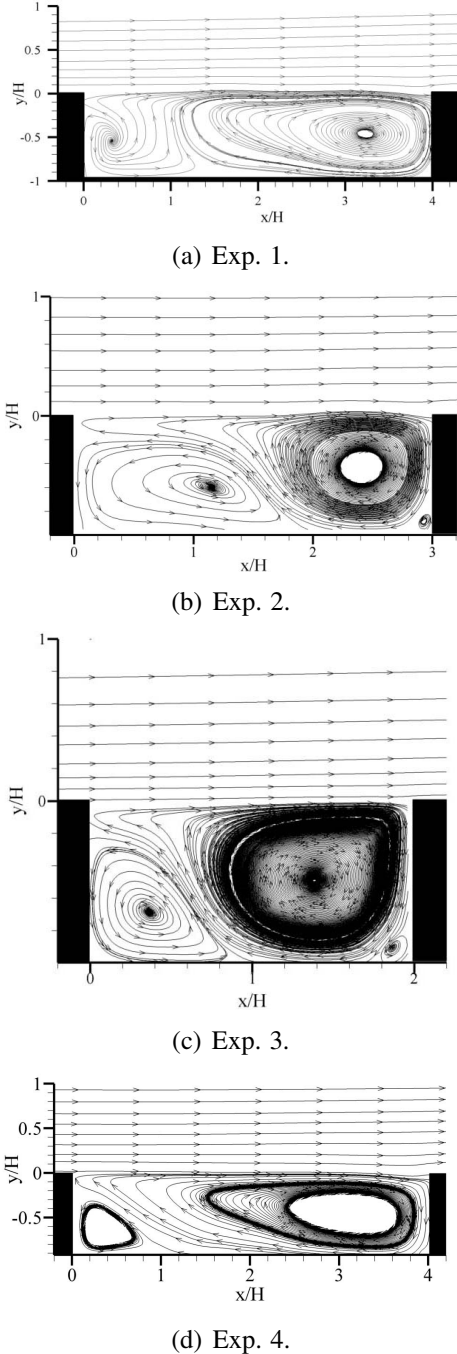


Fig. 5 Mean streamlines; x-y planes.

facing step, and a second separation point near the middle of the cavity bottom wall.

Reducing the cavity aspect ratio as shown in Fig.5b and c, the main recirculation zone covers more and more the whole cavity and a third recirculation zone close to the cavity lower downstream corner grows. This is consistent with findings for cavity aspect ratios of one (see e.g. [7]), where the flow is dominated clearly by the main recirculation zone and two vortices are found in the upstream and downstream corner. The mean velocity fields in planes parallel to the wall at $y=-0.5H$ are shown in Fig. 6a-6d for the different cavities (flow comes from the bottom of the images). The transverse coordinate in the Figures is arbitrary.

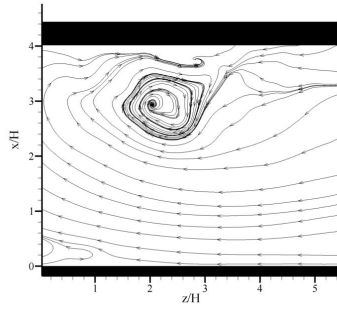
Faure et al. [7] finds by flow visualization jets originating from the cavity lateral confines, which meet in the spanwise center of the cavity. Further, they show that 3-dimensional structures develop along the backward and/or forward facing step, which are relatively steady along the cavity span. Also in the present case, jets originating from the cavity lateral confines are observed (Fig. 6a-c), whereas not always one sees these jets meeting in the center of the field of view like in Fig. 6b. This may be due to slightly different boundary conditions at the two lateral ends of the cavities. The cavity with aspect ratio $L/H=4$ and laminar incoming boundary layer shows a transverse flow going uniquely in one direction in the upstream part of the cavity. The cavity with the turbulent incoming boundary layer (Fig.6d) shows a mean flow which is just slightly directed in spanwise direction. The center of the recirculation zone is also visible. The streamlines of Exp. 3 (Fig.6c) show a transverse flow in one direction for the whole field.

In Fig. 6a a recirculation zone is seen close to the forward facing step, indicating the presence of a flow structure in this area. Also in Fig. 6b it is seen that the streamlines meet in a point in the center of the field of view, possibly indicating a 3-dimensional effect. The same streamline pattern as in Fig. 6b is found from the tomographic PIV measurements of Exp. 6 (here not shown). The mean streamline plots give a first indication of 3-

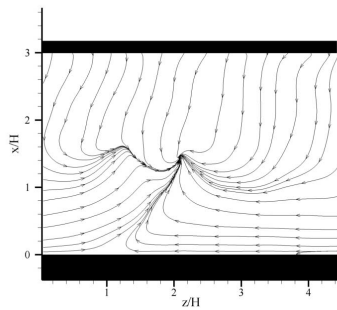
INVESTIGATION OF THE FLOW IN A RECTANGULAR CAVITY USING TOMOGRAPHIC AND TIME-RESOLVED PIV

dimensional structures present inside the cavity, which will be investigated more in detail in section 3.2.2.

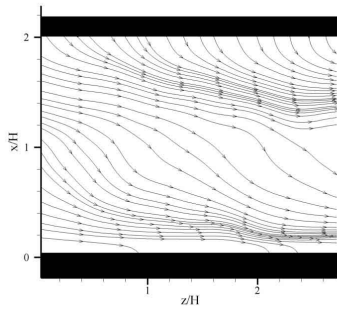
The peak levels of the shear component of the



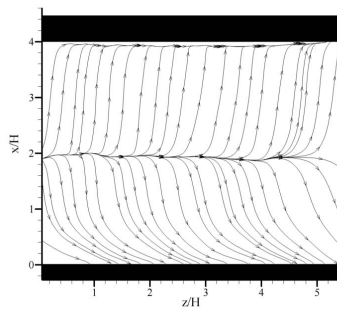
(a) Exp. 1.



(b) Exp. 2.

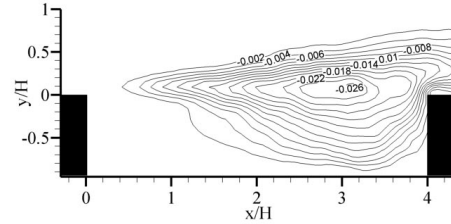


(c) Exp. 3.

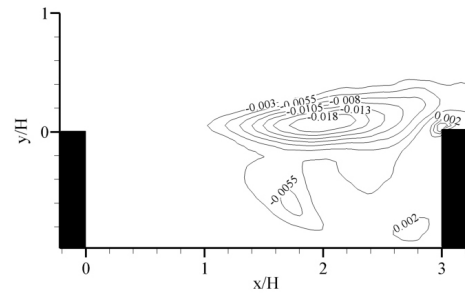


(d) Exp. 4.

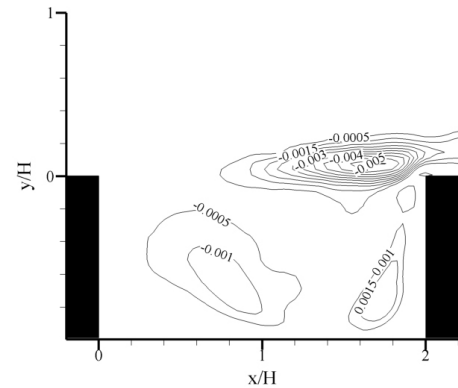
Fig. 6 Mean streamlines; x-z planes.



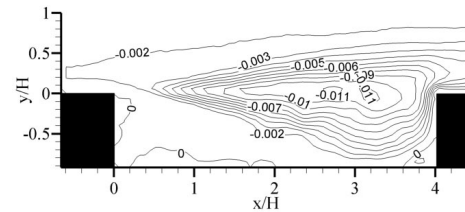
(a) Exp. 1.



(b) Exp. 2.



(c) Exp. 3.



(d) Exp. 4.

Fig. 7 Normalized Reynolds stress $\overline{u'v'}/U_e^2$.

Reynolds stress (Fig.7) shows much higher values for the cavities with aspect ratio 4 and especially with a laminar incoming boundary layer ($\overline{u'v'}/U_e^2 = -0.026$ in Fig. 7a) than with a turbu-

lent incoming boundary layer ($\overline{u'v'}/U_e^2 = -0.011$ in Fig. 7d). Reducing the aspect ratio with the laminar incoming boundary layer (Fig.7b and 7c) the maximum Reynolds shear stress reduces to -0.018 and -0.005, respectively. The location of the maxima in all four cases is at about 3/4L downstream of the cavity backward facing step.

The time averaged development of the shear

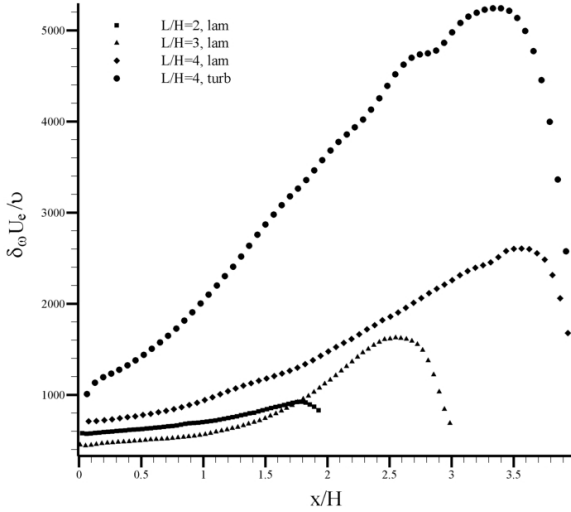


Fig. 8 Vorticity thickness δ_ω .

layer along the cavity mouth can be described by the vorticity thickness, defined as

$$\delta_\omega(x) = \frac{U_2 - U_1}{\left(\frac{\partial \overline{U}}{\partial y}\right)_{max}}$$

where, here, U_2 is the cavity external flow velocity and $U_1 = 0$. Fig. 8 shows the variation of $\delta_\omega(x)$, normalized with U_e/ν . The data show a linear growth of the shear layer for the cavity with the turbulent incoming boundary layer over almost the entire length of the cavity, with a spreading rate $\frac{d\delta}{dx} = 0.3$. Instead, the cavities with the laminar incoming boundary layer show a mean spreading rate lying between $0.1 < \frac{d\delta}{dx} < 0.2$, where it has to be noticed that this rate shows to be dependent on the position along the cavity mouth. A mean convection velocity of the flow structures in the shear layer can be determined by 2-point temporal correlation of the longitudinal

fluctuating velocity for different positions along the cavity mouth. The time lag found by the correlation in connection with the distance between the two points, used for the correlation, gives a convection velocity of around 45% of the free stream velocity for the cavity with the turbulent incoming boundary layer and of about 60% of the freestream velocity with the laminar boundary layer. The fact that the cavity with the turbulent incoming boundary layer shows a lower vortex convection velocity than the other cavities is due to the large thickness of the boundary layer.

3.2 Time resolved results

3.2.1 x-y Planes

Figs.9a-9d shows instantaneous snapshots of the four different cavities over a vortex shedding period T , where the color plot represents the vorticity normal to the plane and the isolines identify vortices using the λ_{ci} vortex identification criterion, where λ_{ci} is the swirling strength as introduced by Zhou et al. [31](1999). The λ_{ci} criterion was here mainly applied to identify large scale structures and before computing the velocity gradient tensor (using a central difference scheme of second order) a polynomial special filter of second order with a 5×5 grid point stencil was applied to the PIV data. Moreover, from the present 2-dimensional data, only the projection of the full 3D velocity gradient tensor to the measurement plane can be calculated, which may cause uncertainties in identifying vortices, when their axes are far to be normal to the measurement plane. Therefore, the swirling motions selected for analysis and comments were validated by the presence of a peak of vorticity in the center of each λ_{ci} contour and by the observation of a spiral motion in the vector velocity field, when seen in a frame of reference traveling with the vortices (practically subtracting a velocity corresponding or nearly corresponding to the vortex convective velocity).

As shown in detail in [12], the cavity with the turbulent incoming boundary layer is characterized by a less organized flow pattern. Vortices are shed from the cavities leading edge irregularly,

INVESTIGATION OF THE FLOW IN A RECTANGULAR CAVITY USING TOMOGRAPHIC AND TIME-RESOLVED PIV

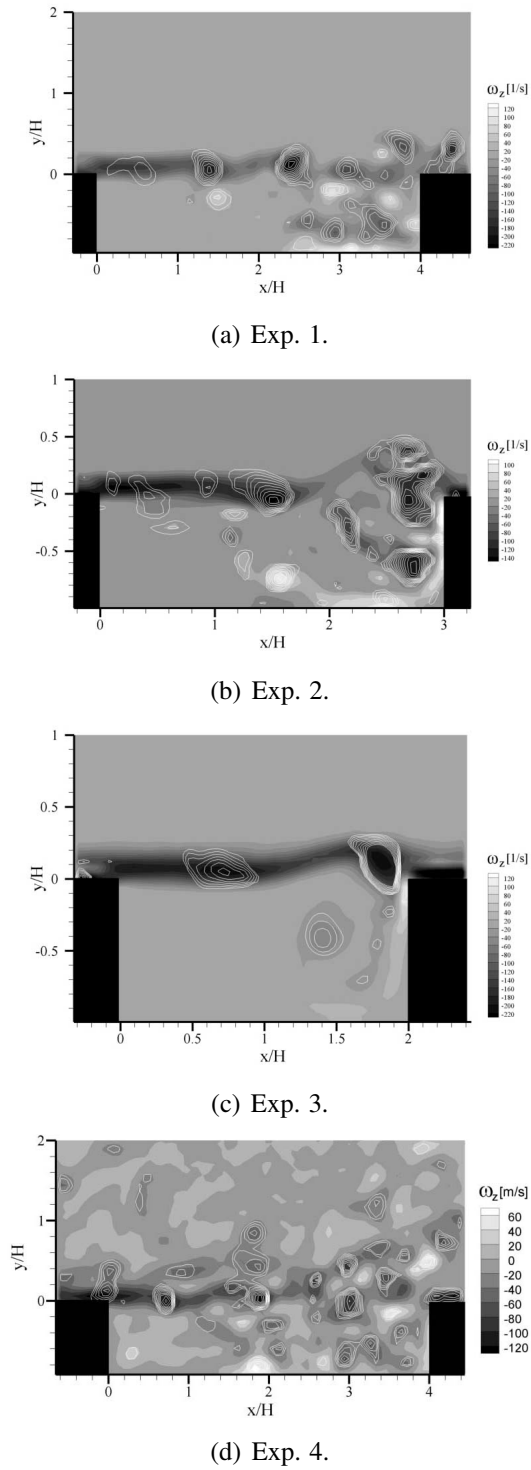


Fig. 9 Instantaneous vorticity fields ω_z (color plot) and λ_{ci} (isolines).

which is due to the thick incoming boundary layer. It influences on one side the Kelvin-Helmholtz instability mechanism in the cavity shear layer and on the other side it introduces turbulent flow structures, which continue to exist inside the cavity shear layer and which are seen in the instantaneous snapshots. An example is shown in Fig. 9d. However, by observing a time sequence of the flow, one notices that there is a periodic inflow and outflow into and out of the cavity related to a filling up and breakdown of the main recirculation zone. This leads to a low frequency oscillation ($St_L \approx 1.5$) of the flow in the cavity, which is seen in the spectrum of the wall-normal velocity at a point in the shear layer close to the cavity trailing edge (see Fig.10) and the spectrum of the time history of the instantaneous drag coefficient at the same point (see [12]).

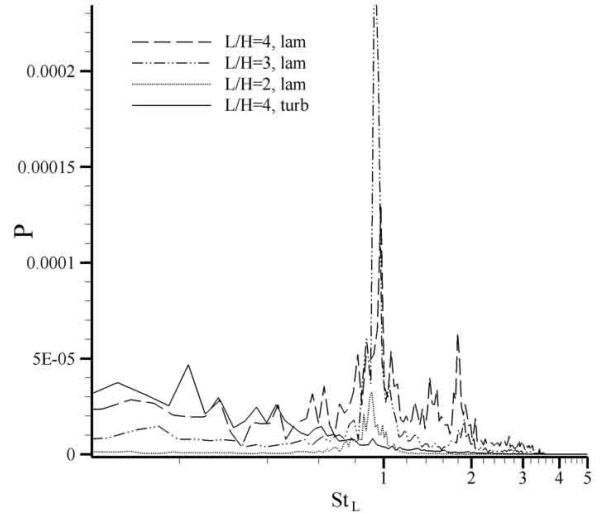


Fig. 10 Power spectrum of wall-normal velocity.

Observing a time sequence of snapshots like in Fig. 9a-9c, the difference to the flow as in Fig. 9d is evident. The ratio of L/θ is higher than in Exp. 4, even if this ratio is not greater than 80 as claimed by Grace et al [11] as an indication for the onset of oscillations in a cavity flow. In Exp. 1, a regular vortex shedding takes place in the shear layer. This regular vortex shedding leads

to a peak at $St_L = 0.95$ in the spectrum of the wall normal velocity at a point in the shear layer close to the cavity trailing edge. A second peak in the spectrum of this cavity is found at $St_L = 1.9$ representing a harmonic of the first mode.

It is also seen by a visual observation of a sequence of snapshots, that the main recirculation zone still influences the shear layer in the downstream part of the cavity for the cavity with aspect ratio $L/H=4$ (Exp. 1). This influence can be observed in the velocity spectrum (Fig. 10), which shows a higher energy content at low St_L . As mentioned above, also the spectrum of the cavity of Exp. 4 had a higher fluctuating energy level at a Strouhal number St_L of about 0.2.

Reducing the cavity aspect ratio (Exp. 2 and 3 in Fig.9), the energy content at low Strouhal number disappears.

3.2.2 3D flow organization

As mentioned above, it is postulated that the shear layer of the cavity of Exp. 4 ($L/H=4$, turbulent) is populated by vortices originating from a Kelvin-Helmholtz instability in the shear layer, and also by structures, which originate from the turbulent incoming boundary layer. The latter can be supported by observing the flow using planar time-resolved PIV in a plane parallel to the wall just slightly above the cavity mouth ($y/H \approx 0.03; y^+ = 40$) as shown in Fig. 12 in [12]. In Haigermoser et al. is seen that these structures, coming from the boundary layer, can be tracked during their way inside the shear layer. Assuming that these turbulent boundary layer structures have a hairpin like shape as it was shown by many studies (e.g. [28] and [16]), they must be seen in the x-y planes and lead to the irregular vortex pattern of Fig. 9d. This observation is supported by instant images of Exp. 5 (Fig. 11), where the flow of a rectangular cavity with the parameters as in Table 1 is shown. The data includes the 3 components of the velocity in a volume covering the whole cavity mouth from $-5mm < y < 5mm$. Fig. 11 shows iso-surfaces of the absolute vorticity with a value of $|\omega| = 4900$ 1/s and a slice through the volume parallel to the wall at $y = 0$, where

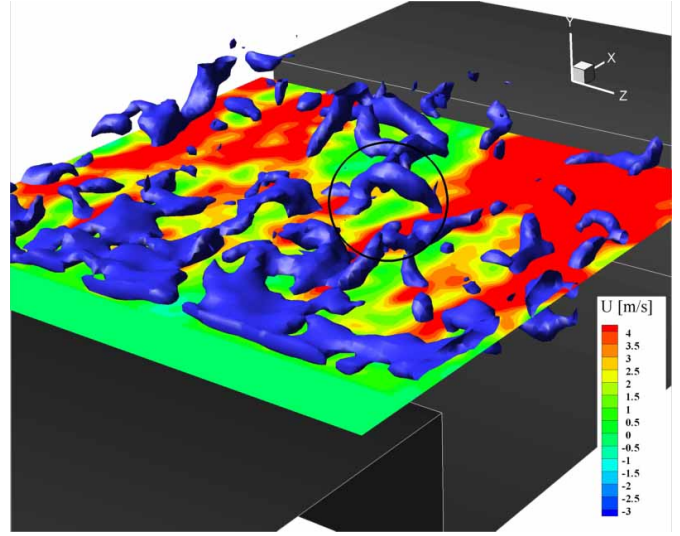


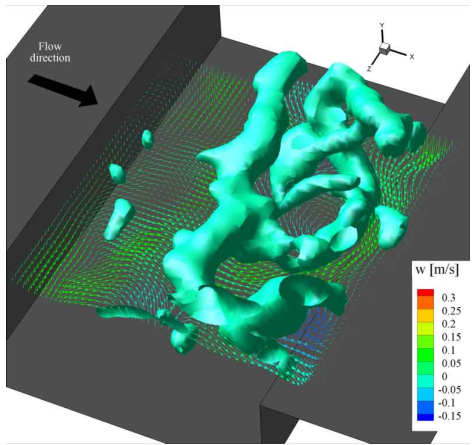
Fig. 11 Snapshot of vorticity iso-surfaces and slice in the x-z plane at $y=0$; color plot in slice codes the streamwise velocity.

the color codes the streamwise velocity. The circle points out a structure in the flow which has the form of a hairpin. Between the arms of the hairpin vortex, a zone of low streamwise momentum is seen, reflecting characteristics of hairpin structures existing in a turbulent boundary layer. Therefore, in connection with the planar time-resolved results in the x-y and x-z planes, it is shown that the turbulent flow structures from the incoming boundary layer continue to exist inside the shear layer until relatively far downstream of the cavity leading edge.

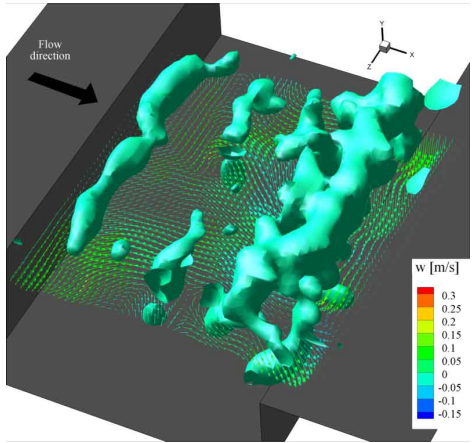
In contrary to the study by Faure et al. [7] (2007), no organized 3D structures were found inside the cavity with the turbulent incoming boundary layer, but a rather chaotic instantaneous flow was found (see Fig. 12 [12] and Fig. 9d).

The 3D flow in the cavity with the laminar incoming boundary layer (Exp. 6) was investigated using time resolved tomographic PIV. First, a sequence of 3 snapshots showing iso-surfaces of $\lambda_{ci} = 251/s$ is presented in Fig. 12 in order to examine the shear layer characteristics. Additionally a x-z slice through the velocity vector field is shown at $y=-0.3H$, where the vector color codes the spanwise velocity w . Vortex tubes can be observed in spanwise direction, developing in the shear layer due to a Kelvin-Helmholtz instabil-

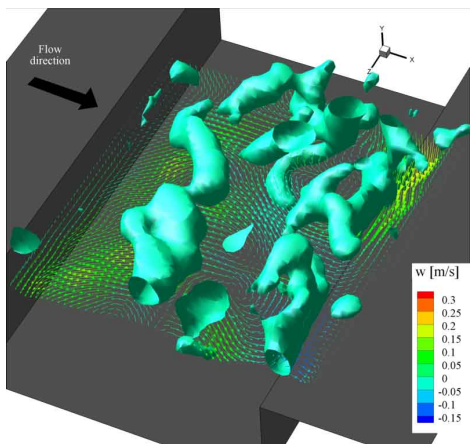
INVESTIGATION OF THE FLOW IN A RECTANGULAR CAVITY USING TOMOGRAPHIC AND TIME-RESOLVED PIV



(a) t_0 .



(b) $t_0 + T/2$.



(c) $t_0 + T$.

Fig. 12 $\lambda_{ci} = 25$ 1/s iso-surfaces and x-z slice through velocity vector field at $y=-0.3H$.

ity. These tubes assume a rather 3D shape especially more downstream from the leading edge. They loose coherence and significant magnitudes of vorticity is found successively in all components (here not shown). This may be due to the influence of the flow inside the cavity and especially the main recirculation zone, as it was shown in section 3.2.1. The 3D organization of the flow is illustrated with the slice through the velocity vector field in Fig. 12, where a stronger flow in upstream direction is found at both side of the field of view compared to the central area. This indicates the presence of a structure in this part of the flow, which may influence the shear layer development. Faure et al. [7] (2007) observed such structures and noted that the move slightly from the cavity center towards the spanwise ends. The time scale of such a movement is very high compared to the acquisition time of the present measurement. A non-converged average velocity field and successively the 3D streamlines were computed from the present time-resolved results in order to visualize the 3D structure inside the cavity (Fig.13). The color of the streamlines in Fig. 13 indicates the spanwise velocity w . It is seen that the streamlines indicate a slight outflow from the cavity in the center of the field of view and an inflow on the sides. Due to this inflow the downstream recirculation zone is larger on the sides than in the center and also the above described jets at the lateral ends of the field of view, originating from the forward facing step and reaching the backward facing step, can be explained. Further, from Fig. 13 one can imagine the core line through this recirculation zone which assumes the shape of a large hair-pin or horseshoe. The structure observed here may be the same as the ones observed by Faure et al. [7] (2007), where a direct comparison is difficult as in the present case we observe quasi-mean streamlines and in the smoke visualization of Faure et al. [7] (2007) pathlines are seen in a plane parallel to the wall.

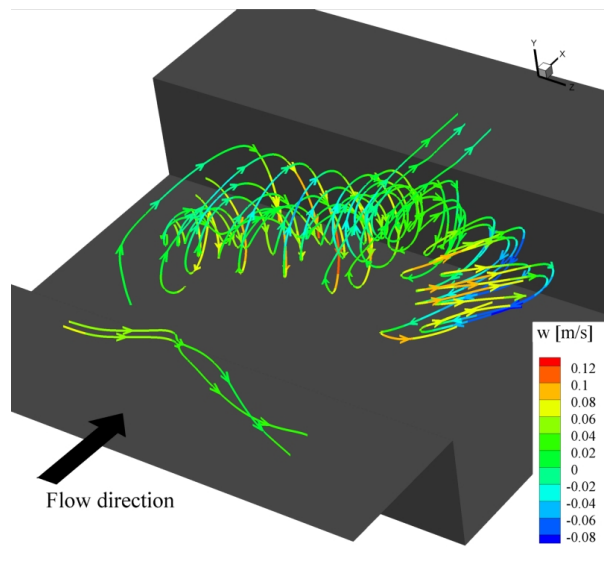


Fig. 13 3D streamlines of the averaged velocity field; color codes the spanwise velocity w .

4 Conclusions

The flow in rectangular cavities at very low Mach number with a thick turbulent incoming boundary layer and with laminar boundary layer was investigated using data from time-resolved planar and tomographic PIV. No self-sustained oscillations were found in the case of the thick turbulent boundary layer, due to the high value of the thickness of the incoming boundary layer and the low ratio of L/θ . It was seen by planar PIV measurements in a plane parallel to the wall and by tomographic measurements of the cavity shear layer, that the flow is strongly influenced by the turbulent boundary layer. It impacts on the instability mechanism in the shear layer and introduces turbulent structures which continue to exist inside the shear layer.

The cavities with the laminar incoming boundary layer show a principle oscillation Strouhal number of $St_L=0.95$, corresponding to a regular vortex shedding from the leading edge of the cavities due to a Kelvin-Helmholtz instability. It is seen that for the larger aspect ratios L/H , the shear layer is influenced by the main recirculation zone in the cavity downstream part. Time-resolved tomographic PIV measurements of the flow in a cavity with a aspect ratio of $L/H=3$ and a lami-

nar incoming boundary layer allowed to observe the behavior of the vortex shedding in the shear layer, which was seen to be rather 3-dimensional. Especially in the cavity downstream part, the vortex tubes assume a lower spanwise organization, which may be due to the presence of a quasi steady 3D-structure as shown in the averaged streamline plot. This structure assumes a kind of horseshoe shape, forcing the fluid to exit the cavity in one area (center of the field of view here) and entering aside.

The main noise generating mechanism in a cavity is the impingement of vortices shed in its shear layer onto the forward facing step. The spanwise modes inside the cavity do not generate noise directly, but they may influence the noise generating mechanism and therefore also indirectly the sound emission. This paper is a contribution to understanding the spanwise organization of the flow.

5 Acknowledgments

The study was carried out within a Marie Curie Early Stage Training framework (EST).

6 Copyright Issues

The copyright statement is included in the template and must appear in your final pdf document in the position, style and font size shown below.

7 Copyright Statement

The authors confirm that they, and/or their company or institution, hold copyright on all of the original material included in their paper. They also confirm they have obtained permission, from the copyright holder of any third party material included in their paper, to publish it as part of their paper. The authors grant full permission for the publication and distribution of their paper as part of the ICAS2008 proceedings or as individual off-prints from the proceedings.

References

- [1] Adrian R.J., Hairpin vortex organization in wall turbulence, *Physics of Fluids*, Vol. 19, 2007.

INVESTIGATION OF THE FLOW IN A RECTANGULAR CAVITY USING TOMOGRAPHIC AND TIME-RESOLVED PIV

- [2] Ashcroft G. and Zhang X., Vortical structures over rectangular cavities at low speed, *Physics of Fluids*, Vol. 17, 2005.
- [3] Bilanin A.J. and Covert E.E., Estimation of possible excitation frequencies for shallow rectangular cavities, *AIAA J.*, Vol. 11, pp. 347-351, 1973.
- [4] Chatellier L., Laumonier J., Gervais Y., Theoretical and experimental investigations of low Mach number turbulent cavity flows, *Exp Fluids*, Vol. 36(5), pp. 728-740, 2004.
- [5] Elsinga G. E., Van Oudheusden B.W., Scarano F., Experimental assessment of tomographic-PIV accuracy, 13th international symposium on applications of laser techniques to fluid mechanics, Lisbon, Portugal, paper 20.5, 2006.
- [6] Elsinga G. E., Scarano F., Wieneke B., van Oudheusden B. W., Tomographic particle image velocimetry, *Exp Fluids*, Vol. 41, p. 933-947, 2006.
- [7] Faure T. M., Adrianos P., Lusseyran F., Pastur L., Visualizations of the flow inside an open cavity at medium range Reynolds numbers, *Exp Fluids*, Vol. 42, pp. 169-184, 2007.
- [8] Ganapathisubramani B., Hutchins N., Hambleton W.T., Longmire K., Marusic I., Investigation of large-scale coherence in a turbulent boundary layer using two-point correlations, *J. Fluid Mech.*, Vol. 524, pp. 57-80, 2005.
- [9] Gharib M. and Roshko A., The effect of flow oscillations on cavity drag, *J. Fluid Mech.*, Vol. 177, pp. 501-530, 1987.
- [10] Ghia U., Ghia K.N., Skin C.T., High-re solutions for incompressible flow using the navier-stokes equations and a multigrid method, *J. Comput. Phys.*, Vol. 48, pp. 387-411, 1982.
- [11] Grace S.M., Dewar W. G., Wroblewski D.E., Experimental investigation of the flow characteristics within a shallow wall cavity for both laminar and turbulent upstream boundary layers, *Experiment in Fluids*, Vol. 36, pp. 791-804, 2004.
- [12] Haigermoser C., Vesely L., Novara M., Onorato M., A time-resolved PIV investigation of a cavity flow with a thick incoming turbulent boundary layer, submitted to *Physics of Fluids*, 2008.
- [13] Howe M.S., Low strouhal number instabilities of flow over apertures and wall cavities, *J. Acoust. Soc. Am.*, Vol. 102, pp. 772-780, 1997.
- [14] Jeong J., Hussain F., Schoppa W., Kim J., Coherent structures near the wall in a turbulent channel flow, *J. Fluid Mech.*, Vol. 332, pp. 185-214, 1997.
- [15] Komerath N.M., Ahuja K.K., Chambers F.W., Prediction and measurement of flows over cavities, *AIAA 25th aerospace sciences meeting*, 1987.
- [16] Lagraa B., Labraga L., Mazouz A., Characterization of low-speed streaks in the near-wall region of a turbulent boundary layer, *European Journal of Mechanics B/Fluids*, Vol. 23, pp. 587-599, 2004.
- [17] Larsson J., Davidson L., Olsson M., Eriksson L., Aeroacoustic Investigation of an Open Cavity at Low Mach Number, *AIAA Journal*, 0001-1452 vol.42 no.12, pp. 2462-2473, 2004.
- [18] Lin J.C. and Rockwell D., Organized oscillations of initially turbulent flow past a cavity, *AIAA J.*, Vol. 39, pp. 1139-1151, 2001.
- [19] Ozsoy E., Rambaud P., Stitou A., Riethmuller M.L., Vortex characteristics in laminar cavity flow at very low Mach number, *Experiment in Fluids*, Vol. 38, pp. 133-145, 2005.
- [20] Palmiotti G., Experimental analysis of cavity flows, Master thesis at the Politecnico di Torino, Italy, 2006.
- [21] Powell A., On edge tones and associated phenomena, *Acustica*, Vol. 3, p. 233-243, 1953.
- [22] Powell A., On the edge tone, *J. Acoust. Soc. Amer.*, Vol. 33 (4), p. 395-409, 1961.
- [23] Rockwell D. and Naudasher E., Review-self-sustaining oscillations of flow past cavities, *J. Fluid Eng.*, Vol. 100, pp. 152-165, 1978.
- [24] Rossiter J. E., Wind-tunnel experiments on the flow over rectangular cavities at subsonic and transonic speeds, *Aero. Res. Council.*, 1964.
- [25] Rowley C.W., Colonius T., Basu A.J., On self-sustained oscillations in two-dimensional compressible flow over rectangular cavities, *J. Fluid Mech.*, Vol. 455, pp. 315-346, 2002.
- [26] Sarohia V., Experimental investigation of oscillations in flows over shallow cavities, *AIAA J.*, Vol. 15, p. 984-991, 1977.
- [27] Sarohia V., Massier P. F., "Control of Cavity Noise," *J Aircraft*, Vol. 14, p. 833-837, 1977.

- [28] Tomkins C.D., Adrian R.J., Spanwise structure and scale growth in turbulent boundary layers, *J. Fluid Mech.*, Vol. 490, pp. 37-74, 2003.
- [29] Tomkins C.D., Adrian R.J., Spanwise structure and scale growth in turbulent boundary layers, *J. Fluid Mech.*, Vol.490, pp. 37-74, 2003.
- [30] Ukeley L. and Murray N., Velocity and surface pressure measurements in an open cavity, *Experiment in Fluids*, Vol 38, pp. 656-671, 2005.
- [31] Zhou J., Adrian R.J., Balachandar S., KendallT.M., Mechanisms for generating coherent packets of hairpin vortices in channel flow, *J. Fluid Mech.*, Vol. 387, pp. 353-396, 1999.